Chapter 3

The Pulsed Resistive Low-Field MR Scanner

3.1 Background

In the remaining part of this work we are going to describe hyperpolarized gas relaxation, diffusion and MR imaging experiments. These experiments were performed on a pulsed resistive low-field scanner that was constructed at Stanford University for low-field high-resolution imaging of water using the "prepolarized MRI" technique (or PMRI). In this chapter, we motivate the construction of a hybrid hyperpolarized gas/proton MRI scanner by exploring signal-to-noise (SNR) properties of hyperpolarized gas and prepolarized water during MRI. In addition, we describe the principles behind prepolarized water MRI, the pulse sequence used in the PMRI experiments and the electronics components of the pulsed resistive low-field scanner.

Conventional MRI techniques require a magnetic field that is both strong and homogeneous. The strength of the field determines the extent of magnetization induced in the sample, while the variation in the field (i.e, inhomogeneity) has to be smaller than the size of the gradients used during imaging. Such fields are usually produced by large and heavy static magnets or by cryogenically cooled and thus expensive superconductors. An alternative approach is the prepolarized MRI technique in which two separate pulsed fields produced by two different magnets–a polarizing magnet and a readout magnet–assume the role of the conventional $B_\circ$ field [62, 25].

In PMRI, the polarizing magnet produces a strong (0.35 T) yet inhomogeneous magnetic field which determines the sample's magnetization, and consequently, the signal-to-noise ratio (SNR) of the MR image. The 20% inhomogeneity of the magnet causes the net

magnetization to vary across the sample. However, such variations are gradual and smooth, and since human vision is insensitive to smooth variations of this order, the MR image quality is not affected by the inhomogeneity of the polarizing magnet. In fact, clinicians now routinely image with variations of several hundred percent when using surface coils.

The readout magnet produces a relatively weak (0.025 T) yet homogeneous field which is applied after the spins have been polarized by the polarizing field to produce the Larmor precession of spins needed for MR detection. Unlike the polarizing field, the readout field has to be extremely homogeneous, since dispersion in the Larmor frequency of a spin ensemble leads to spin de-coherence (i.e, dephasing) and thus to MR signal loss. On the other hand, the strength of the readout field has no effect on the SNR of the image, provided the sample completely loads the RF coil. Therefore, the readout field needs only to be large enough to dominate the Earth's field and thus to provide an axis of magnetization for the precessing spins.

In order to combine the polarizing and the readout magnet into a single MR scanner–which would allow for a polarizing and a readout phase in the pulse sequence–the two electromagnets have to operate as pulsed, rather than as static magnets. It is this pulsed (or field-cycled) property of the system that makes building such a system technically challenging [25]. In addition, the energy stored in the polarizing field must be small enough to facilitate field-cycling, so the PMRI concept is most applicable for imaging relatively small samples, such as human extremities (knee, head, hands) [24]. Finally, the excessive power dissipation (greater than 10 kW) poses additional challenges at readout fields above 0.35 T.

One of the potential advantages of the PMRI (i.e, low-field pulsed resistive) system is that the pair of resistive electromagnets can be manufactured at a greatly reduced cost as compared to a single superconducting magnet. This has the potential to make routine imaging, which is necessary in disease control and treatment monitoring, more feasible as well as accessible to a larger fraction of the population. Furthermore, because of the low readout field strengths used, the PMRI system has all the advantages of a low-field scanner, such as smaller susceptibility effects and reduced RF power deposition, without the usual cost in image SNR.

However, it is the field-cycled nature of the polarizing and readout fields that holds the most promise for novel MR applications. Changing the strength of the polarizing pulse

enables the investigation of rich T1 dispersion-based MR contrast [63], while varying the strength of the readout pulse makes the system suitable for imaging substances other than water (such as hyperpolarized gases–^{3}He and ^{129}Xe) without the need to re-tune the RF coils.

3.2 Signal-to-Noise Ratio in MRI, PMRI and Hyperpolarized Gas MRI

3.2.1 MR Signal

The source of MR signal is the precession of nuclear magnetization in a $B_\circ$ field. The transverse component of the precessing magnetization induces a voltage at the receiver coil input according to Faraday's law of induction. To quantify this signal, we can look at the magnetization in a voxel of size dV, $\mathbf{M}(t,\mathbf{r})dV$, placed at a point P away from a conductor. The time-varying magnetization induces a voltage V(t) in the conductor. If instead, the conductor carried a current I(t), it would produce a magnetic field of size $\mathbf{B_1}$ at point P. Employing the Lorentz Reciprocity theorem [23, 22], it can be shown that

$$\mathrm{V(t)} \otimes \mathrm{I(t)} = -\int_V \mathbf{B_1} \otimes \frac{\partial \mathbf{M}(t,\mathbf{r})}{\partial t}\, dV \tag{3.1}$$

The solution to the rotating magnetization can be represented in complex notation as

$$\mathbf{M}(t,\mathbf{r}) = \mathbf{M}_\circ \{exp(-i\omega t) + \text{other terms}\}, \tag{3.2}$$

where $\mathbf{M}_\circ$ is the nuclear magnetization, ω is the Larmor frequency of precession, and "other terms" could represent the T_2 relaxation (decay) of the transverse component, $exp(-t/T_2)$, or precession in an imaging gradient $\mathbf{G}$, $exp(-i\gamma \int \mathbf{G}(\tau)\cdot\mathbf{r}d\tau)$.[1] The nuclear magnetization is given (in SI units) by

$$\mathbf{M}_\circ = N\gamma^2\hbar^2 I(I+1)\mathbf{B}_\circ/3kT, \tag{3.3}$$

where N is the number of spins at resonance per unit volume, γ is the gyromagnetic ratio of nuclei and T is the temperature of the sample. If we insert Eq. 3.2 into Eq. 3.1 and then differentiate with respect to time, we get

$$s(t) = -i\omega B_1 M_\circ\, exp(-i\omega t)\, dV, \tag{3.4}$$

[1] These terms are avoided because they are irrelevant in the present derivation.

where we assumed unit current I(t) and replaced the voltage symbol V with $s(t)$ to describe the NMR signal. If the NMR signal is averaged over the acquisition time, then

$$S \propto \omega B_1 M_\circ \, dV \sqrt{T_{acq}}. \tag{3.5}$$

In conventional MRI, the frequency of precession and the magnetization of the sample are both proportional to the applied field $B_\circ$ ($\omega \propto B_\circ$, $M_\circ \propto B_\circ$), so that the NMR signal varies as the square of the $B_\circ$ field,

$$S_{MRI} \propto B_\circ^2 B_1 \, dV \sqrt{T_{acq}}. \tag{3.6}$$

On the contrary, in PMRI, the readout field B_r determines the Larmor frequency of precession, so that $\omega \propto B_r$, while the polarizing field B_p determines the sample's magnetization, $M_\circ \propto B_p$. Therefore, the signal of prepolarized water is linear in both the polarizing and the readout magnetic field strengths:

$$S_{PMRI} \propto B_r B_1 B_p \, dV \sqrt{T_{acq}}. \tag{3.7}$$

Like prepolarized water, hyperpolarized noble gas magnetization is not a function of the readout field strength; rather, it is determined by the efficiency of the optical pumping and the spin-exchange processes which are used to polarize the nuclear spin of the noble gas (see Chapter 2). As in PMRI, Larmor frequency is determined by the strength of the readout field B_r. The hyperpolarized gas MR signal is then proportional to

$$S_{HypGas} \propto B_r B_1 \mu_\circ M_{gas} \, dV \sqrt{T_{acq}}, \tag{3.8}$$

where M_{gas} represents the gas magnetization and $\mu_\circ$ is the permeability of free space.

3.2.2 Noise in MRI

The main source of noise in MR arises from random electrical fluctuations created by Brownian motion of electrons in a conductor. Such noise (also called "resistive" or Johnson noise) is thermal in origin, adds linearly to the signal and can be modelled as Gaussian-distributed.

The mean square voltage induced by the random motion of electrons in a conductor of

resistance R, temperature T and bandwidth Δf is[2]

$$\langle \mathrm{V}^2 \rangle = 4kTR\Delta f. \tag{3.9}$$

Because Johnson noise is due to random processes, the average noise voltage is zero. Therefore, to account properly for random noise sources in MR, one has to consider the RMS (root-mean-square) values of noise. When uncorrelated, the noise power from different thermal sources has to be added.

There are two main sources of thermal noise in MRI: the receiver coil (with resistance R_c), and the body (or sample) as seen by the receiver coil (with resistance R_s). In general, the coupling between the body and the receiver coil is inductive as well as capacitive. However, only inductive coupling is required for MR signal detection.[3] The capacitive coupling occurs when quasi-static electric fields produced by the coil penetrate the body. Since capacitive coupling in tissue creates an additional resistive noise source, it should be minimized through proper design and shielding of RF coils.

To determine the variation of noise with frequency, one needs to examine how the coil and the body resistance vary with the frequency of transmission. The body resistance R_s varies as the square of Larmor frequency [22]. The coil resistance, on the other hand, depends on factors such as resistivity of the conductor, coil geometry (coil radius and the number of turns), proximity fields and skin depth of the conductor at the particular radio frequency [23]. Since the coil resistance is inversely proportional to its skin depth, and skin depth is proportional to $f_\circ^{-1/2}$, the coil resistance grows as $f_\circ^{1/2}$. Summarizing,

$$\begin{aligned} N_s &\propto \sqrt{\langle V^2 \rangle_s} \propto \sqrt{f_\circ^2} \\ N_c &\propto \sqrt{\langle V^2 \rangle_c} \propto \sqrt{f_\circ^{1/2}}, \end{aligned} \tag{3.10}$$

where N_s is the noise induced by the sample, while N_c is the noise induced by the coil.

Apart from the body and coil noise, there are other sources of noise, such as the noise coming from the receiver preamplifier, the matching network, and other electronics. However, under normal operational conditions, these noise sources should be negligible compared to the body and coil noise.

[2]Since the power density (i.e., power per bandwidth, $P/\Delta f$) is independent of the frequency band, the noise is often referred to as "white".

[3]The inductive coupling between the body and the coil produces the MR signal.

3.2.3 SNR in PMRI and Hyperpolarized Gas Imaging

The SNR is defined as the ratio between the signal strength and the noise. Since the signal in MR is measured as a potential difference (i.e., voltage) induced in the receiver coil, the SNR becomes the ratio between the signal voltage and noise voltage. For PMRI, the SNR is derived from Eqs. 3.7 and 3.10,

$$SNR_{PMRI} = \frac{S_{PMRI}}{N_s + N_c} \propto \frac{B_\circ B_p}{\sqrt{\alpha B_\circ^2 + \beta B_\circ^{1/2}}}\,, \tag{3.11}$$

where α and β are proportionality constants coming from Eq. 3.10.

Similarly, for hyperpolarized gas MR, the SNR is derived from Eqs. 3.8 and 3.10,

$$SNR_{Hyp\,Gas} \propto \frac{B_\circ \mu_\circ M_{Xe}}{\sqrt{\alpha B_\circ^2 + \beta B_\circ^{1/2}}}\,. \tag{3.12}$$

One needs to compare the above equations with the expression for the SNR obtained with conventional MRI,

$$SNR_{MRI} \propto \frac{B_\circ^2}{\sqrt{\alpha B_\circ^2 + \beta B_\circ^{1/2}}}\,. \tag{3.13}$$

There are two main SNR regimes in MR imaging, depending on whether the body or the coil is the dominant source of noise. If the imaging frequency is high enough to create significant RF eddy currents, then the body can be the dominant source of noise. This noise regime is called "body-noise dominance". On the other hand, in cases such as low-field imaging or small volume imaging, the receiver coil presents the dominant source of noise. The noise regime is then called "coil-noise dominance". In the body-noise and coil-noise dominant regimes, Eqs. 3.13, 3.12 and 3.11 reduce, respectively, to

Body-noise dominance

$$\begin{aligned} SNR_{MRI} &\propto B_\circ \\ SNR_{Hyp\,Gas} &\propto \mu_\circ M_{Xe} \\ SNR_{PMRI} &\propto B_p\,, \end{aligned} \tag{3.14}$$

Coil-noise dominance

$$\begin{aligned} SNR_{MRI} &\propto B_\circ^{7/4} \\ SNR_{Hyp\,Gas} &\propto B_\circ^{3/4} \mu_\circ M_{Xe} \\ SNR_{PMRI} &\propto B_\circ^{3/4} B_p\,. \end{aligned} \tag{3.15}$$

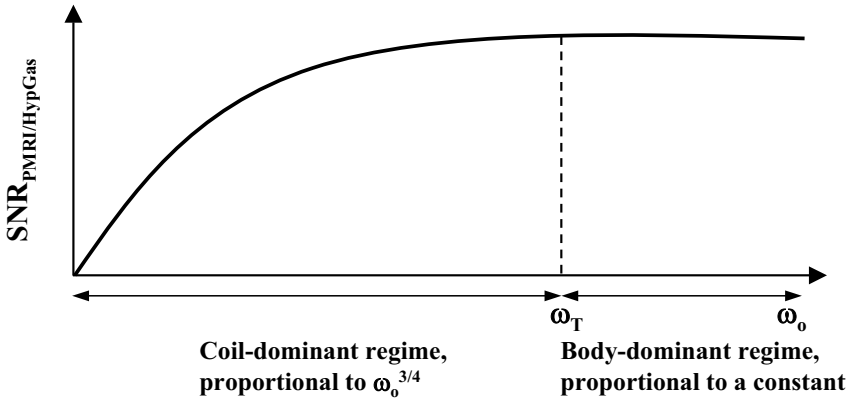

Figure 3.1: SNR as a function of readout frequency for PMRI and hyperpolarized gas MR. The transitional frequency, ω_T, is defined as the frequency at which the coil and the body contribute equal amount of noise. Well below ω_T, the SNR grows as a function of $\omega_\circ^{3/4}$, while well above ω_T, the SNR approaches its asymptotic limit.

The SNR relationships can also be illustrated graphically. Figure 3.1 shows the SNR properties for pre-polarized and hyperpolarized MRI. In the body-noise dominant regime (at readout frequencies at which the noise is dominated by the sample), the SNR of pre-polarized and hyperpolarized gas MRI is independent of the imaging frequency. This means that when body-noise dominance is achieved, there is little benefit to increasing the magnetic field above the transitional frequency (ω_T in the plot).[4] This behavior sharply distinguishes PMRI and hyperpolarized gas MRI from conventional MRI, in which the SNR grows with the strength of the imaging $B_\circ$ field in both noise regimes–a fact which justifies the construction of high-field imaging scanners. In addition, comparing the SNR relationships in Eq. 3.14 for all three imaging modalities, we see that pre-polarized MRI can achieve the same SNR as conventional MRI if the strength of the polarizing field B_p in PMRI is equal to the strength of the imaging field $B_\circ$ in conventional MRI. In other words, the SNR of water which has been pre-polarized with a 0.5 T polarizing pulse should be the same as the SNR of water imaged in a 0.5 T static field scanner.

The strength of the transitional frequency in Figure 3.1 depends on the sample size, conductivity, and the geometry and temperature of the receiver coil. For chest-sized coils

[4] 70% of the SNR lies in the region below the transitional frequency.

used in pulmonary imaging, the transitional frequency is believed to be at or below 1 MHz (30 mT for ^{3}He and 85 mT for ^{129}Xe) [20]. Darrasse *et al.* [47], achieved body-noise dominance at 0.1 T using a body-coil. Magnetic fields of 0.1 T are easily achieved with resistive magnets thus making imaging of pre-polarized water and hyperpolarized gas feasible at low magnetic field strengths without the need for expensive superconductive magnets and without the penalty in SNR.

3.3 PMRI Pulse Sequence

Due to the pulsed nature of the polarizing and readout fields, the pulse sequence for PMRI is more complicated than for conventional MRI. Figure 3.2 shows a typical pulse sequence used in pre-polarized MRI.

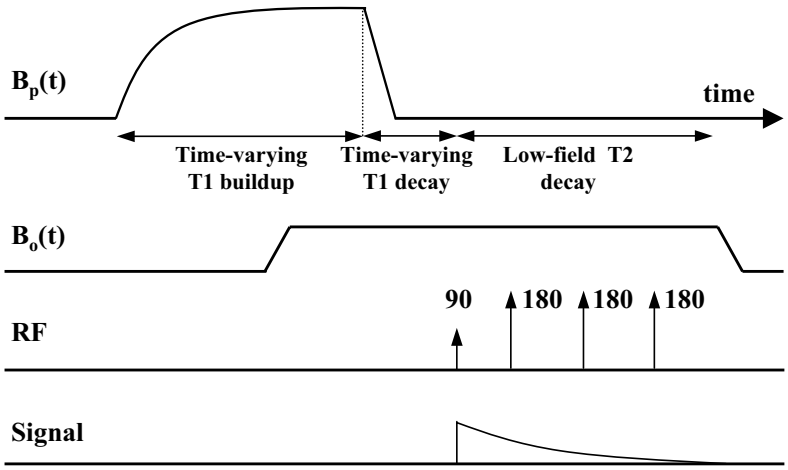

Figure 3.2: Timing diagram illustrating a typical PMRI sequence. B_p is the waveform of the polarizing pulse and $B_\circ$ is the waveform of the readout magnet.

First, a polarizing waveform is applied prior to any RF excitation which governs the build-up of longitudinal magnetization according to the Bloch equation for the z-component of M (written in the rotating frame of reference),

$$\frac{dM_z}{dt} = -\gamma\, M_y\, B_1 + \frac{M_\circ(t) - M_z}{T_1}, \tag{3.16}$$

where $M_\circ(t)$ is the thermal equilibrium polarization at time t defined in Eq. 3.3, but with $B_p(t)$ replacing the $B_\circ$ term; M_z and M_y are the z and y-components of nuclear magnetization at time t; B_1 is the RF field; and T_1 is the longitudinal relaxation time which governs the relaxation of magnetization towards its thermal equilibrium along the z-axis. Equation 3.16 can be simplified by noting that $M_y \approx 0$ throughout the application of the polarizing pulse which is directed along the z-axis. The solution is then

$$M_z = M_\circ(t) + (M_z(0) - M_\circ(t)) \exp\left(\frac{-t}{T_1}\right). \tag{3.17}$$

$M_z(0)$ is the longitudinal magnetization at time $t = 0$, that is, before the onset of the polarizing pulse, when the only magnetic field present is the Earth's field. Since the Earth's field is only 0.5 gauss, $M_z(0)$ is negligibly small and can be ignored.

Note that in PMRI, $M_\circ$ is a function of time, because the polarizing field is a time-varying (i.e., pulsed) field rather than time-independent (i.e., static) field. To solve the above equation exactly, we would need to know the waveform of the polarizing pulse $B_p(t)$. However, if $t >> T_1$, we can assume, to first order, that $M_z = M_\circ(t \rightarrow \infty) \equiv M_p = N\ \mu^2 B_p^{max}/3kT$, where $\mu^2 = \gamma^2\hbar^2\, I(I+1)$. In other words, for sufficiently long polarizing pulses[5], the magnetization achieved can be computed from the maximum (limiting) value of B_p. Since $B_p = 0.5\ T$, the PMRI scanner can achieve a T_1-weighted contrast comparable to mid-field (0.5 T-1.5 T) scanners.

The B_p field must be ramped down to a size smaller than 1 μT (see calculations in Section 3.4.1) before application of the RF pulse and the signal acquisition, otherwise the large (20%) inhomogeneity of the polarizing field will dominate over the imaging gradients, distort the spatial encoding of the object and add phase-shifts. In addition, the quenching of the field must be fast so as to minimize T_1 relaxation during the ramp-down period. Experiments by the Stanford group showed that less than 20% of the magnetization was lost, if the polarizing magnet was ramped down faster than 80 ms [64]. Section 3.4.2 explains how the fast quenching of the field was achieved.

The ramping-down (changing of the current and the magnetic flux) of the polarizing field induces an *emf* (voltage) in the readout magnet, $\epsilon_2 = -\frac{d\Phi_2}{dt} = -M_{21}\frac{dI_1}{dt}$, where ϵ_2 is the *emf* induced in the readout magnet, Φ_2 is the magnetic flux through the readout magnet, M_{12} is the mutual inductance of the magnets (≈ 52 mH), and dI_1/dt is the current change in the polarizing magnet. Since the disturbances in the readout magnet must be below ppm levels (see Section 3.4.1 for detailed calculation), the current in the readout magnet must be controlled precisely using feedback. Switching the readout magnet on before the ramp-down of the polarizing magnet insures that the target field is reached at the end of the ramp-down. Since the self-inductance L of the readout magnet has a stray capacitance C_s and stray resistance R_s associated with it, the disturbances in the readout magnet voltage cause ringing. By implementing critical damping, the ringing time was reduced from 200 ms to less than 15 ms [65].

[5]Typically, $t = 3T_1$ was used in PMRI experiments.

The RF pulse, which tips the magnetization away from the z-axis, can only be applied after the transients subside. Signal acquisition can occur when the dual-mode RF circuitry switches from the transmit to the receive mode. During signal acquisition, only the readout field is present, so the frequency of precession (and acquisition) is governed by the low readout field. Furthermore, the readout field determines the T_2 relaxation rate; however, since T_2 is for most nuclei independent of the magnetic field strength, the PMRI scanner achieves T_2-weighted contrast comparable to high field scanners.

3.4 Electronics of the Pulsed Low-Field Resistive System

3.4.1 Readout Magnet and Power Supply

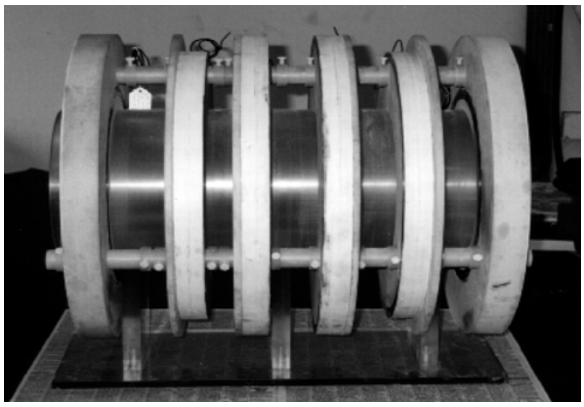

Figure 3.3: Photograph of the homebuild 24 cm bore, 23 mT, 1 kW homogeneous readout magnet for PMRI of extremities. This magnet was used in the hyperpolarized gas experiments.

Ideally, the PMRI readout magnet (Figure 3.3) is designed to operate at a frequency at which the body becomes the dominant source of noise (ω_T in Figure 3.1). The 110 kg homebuild magnet used in the experiments described in this work was designed to operate at 23 mT, but could create a field up to 35 mT, which corresponds to a frequency of 1.49 MHz for water, 415 kHz for ^{129}Xe and 1.14 MHz for ^{3}He. At 23 mT, it required a current of 13 A and dissipated 2 kW of power [25]. Its resistance was 11 Ω, while its self-inductance was 0.34 H. Because the magnet was designed for imaging extremities, it had a 24 cm diameter free bore and a 20 cm spherical homogeneous volume.

As mentioned in Section 3.1, the magnetic field created by the readout magnet must meet stringent stability requirements. In particular, the field must be temporally and spatially stable to ppm levels. The requirement for spatial stability (i.e., magnet homogeneity) is determined by the size of the imaging gradients. For instance, the readout-encoding gradient G needs to be much bigger than the variation in the readout field along the readout (i.e., x) direction:

$$G \gg \frac{\partial \left| B_r(\overrightarrow{r}) \right|}{\partial x}. \tag{3.18}$$

For an imaging frequency of f_r=1 MHz, receiver bandwidth Δf=10 kHz and field-of-view FOV_x=10 cm, the per pixel bandwidth, dx, is 100 Hz/mm. To achieve less than 1 mm

spatial distortion, the readout frequency must deviate by less than 100 Hz, or 100 ppm over the field-of-view.

Similarly, temporal stability of the readout magnet limits the variation in phase to less than π: $\Delta\phi < \pi$. Using the Nyguist theorem, $\Delta x = \pi/\gamma G T_{read}$, this requirement reduces to

$$\Delta B_r < G\Delta x. \tag{3.19}$$

For a 10 kHz receiver bandwidth, a 10 cm FOV_x, and a resolution in x, Δx, of 1 mm, the maximum variation in the readout frequency should be below 100 ppm. However, in addition to field drift, random noise causes phase noise (or field jitter), which can lower the SNR and can often dominate over all other constraints.

While the magnet homogeneity is achieved by a proper magnet design and by utilizing shimming gradients, the temporal stability is a harder condition to fulfill due to the resistive nature of the magnet. When the magnet heats up, the copper wire expands outwards thus changing the magnetic field in the center of the magnet bore and causing a drift in the resonance frequency of the system. When imaging water at 20% duty cycle, the readout frequency drifted 60-80 Hz. To minimize heating, the readout magnet is pulsed on at the end of the polarizing pulse and is pulsed off after the acquisition interval, even though in theory it could be left on during the polarizing phase. The heating of the system can be reduced partially by water-cooling the cooper wires (so called edge-cooling), which will be implemented in the next generation of magnets designed by the Stanford group. Another option, which is easy to implement on the current system, is to design a feedback system which would enable the RF transmitter (and receiver) to follow the frequency drift due to heating.

The pulsed readout magnet power supply is a current source capable of delivering up to 100 A of current. It was built from two *Techron 8607* MRI gradient amplifiers operating in a master-slave mode. The magnet current is sensed and controlled with a *Danfysik Ultrastab* current transducer. In addition, a series resistor-capacitor network in the feedback compensation was adjusted to achieve a critically-damped response to pulsed transients.

Figure 3.4: Photograph of the 13 cm bore, 0.4 T, 10 kW polarizing magnet used for polarizing protons in water in the PMRI experiments.

3.4.2 Polarizing Magnet and Power Supply

The PMRI polarizing magnet used for water experiments described in this work (Figure 3.4), was designed to produce a field strength of 0.4 T while drawing 100 A of current and dissipating 10 kW of power [25]. It weighed 42 kg, had a resistance of 1 Ω and a self-inductance of 65 mH. The diameter of the inner bore was fixed by the size of the object to be imaged, while the outer bore and length were two design variables. For wrist imaging, the inner bore was chosen to be 13 cm, so the magnet was designed to have an outer diameter of 22 cm and a length of 21 cm.

The polarizing magnet has to provide as strong a magnetic field as possible. The field strength is limited by power dissipation. For a magnet of resistance R, carrying a current I, the power P dissipated in the magnet is simply $P = I^2R$. Alternatively, the power can be expressed in terms of the energy U stored in the magnet, where $U = \frac{1}{2}LI^2$, and L is the inductance of the magnet: $P = \frac{2RU}{L}$. The energy stored in the magnet varies with the magnetic field, so that

$$U = \frac{1}{2\mu_\circ} \int_V |\mathbf{B_p}(\mathbf{r})|^2 \, dV, \tag{3.20}$$

where $|\mathbf{B_p}(\mathbf{r})|$ is the magnitude of the polarizing field at position $\mathbf{r}$, and V is the volume containing the field. Substituting Eq. 3.20 into the power equation, yields

$$P = \frac{R}{L} \frac{1}{\mu_\circ} \int_V |\mathbf{B_p}(\mathbf{r})|^2 \, dV. \tag{3.21}$$

Equation 3.21 tells us that the power dissipated in a magnet depends quadratically on the magnetic field amplitude, linearly on the volume of the magnetic field, and inversely on the magnet time constant L/R. Since the time constant varies with the magnet dimension, the

power dissipated will also be a function of magnet size.

Unlike the readout magnet current source, the polarizing magnet current source does not need to supply a precisely regulated current, because the homogeneity requirement for the polarizing magnet is relaxed (see Section 3.1). However, since the current source needs to provide fast high power pulses, it is essential to use fast-switching electronics. The hardest condition to satisfy is the fast ramp-down of the magnetic field. To lose less than 20% of thermal magnetization, the 325 Joules of energy stored in the magnetic field need to be completely dissipated in less than 100 ms [64]. To achieve this, a power switching circuit was designed (Figure 3.5) which effectively transfers the coil energy to a capacitor [66]. When the switch in Figure 3.5 is enabled, current flows into the coil (inductor) and the magnet ramps up. When the switch is disabled, the circuit becomes effectively a parallel resonance RLC circuit. Normally, the energy would oscillate between the inductor and the capacitor with a time constant $T = 2\pi/\omega_\circ = 2\pi\sqrt{LC}$. However, the diodes in the circuit prevent reversal of the current, so the energy gets trapped in the capacitors.

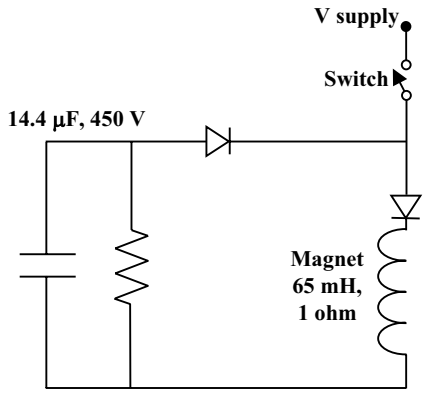

Figure 3.5: The pulsing/switching circuit. The circuit was used to transfer power stored in the conductor into the capacitor.

3.4.3 Transmit-Receive Circuit

PMRI uses low frequency signal detection, which is significantly more challenging than MR signal detection at high frequency. This is in part due to the fact that a higher readout frequency broadens the intrinsic coil bandwidth and in this way relaxes design constraints on the receiver components [24].

Consider a coil which is characterized by its quality factor Q. The Q-factor is equal to the ratio between the energy stored in the coil and the energy dissipated per unit cycle. The smaller the damping, the larger the Q-factor. A high Q coil has a long time response because the damping is small. In terms of the coil's inductance L_c and the series resistance R the Q-factor is

$$Q = \frac{\omega_\circ L_c}{R} \approx \frac{\omega_\circ}{|\Delta\omega|}, \tag{3.22}$$

where $\Delta\omega$ is the width of the resonance and the approximation is true if $\frac{\Delta\omega}{\omega_\circ} \ll 1$. The series resistance R is either equal to R_s when the sample is the dominant source of noise, or R_c when the coil is the dominant source of noise. Therefore, from the above equation it follows that

$$\begin{aligned} \Delta\omega &\propto \omega_\circ^2 \quad \text{when } R \approx R_s \\ \Delta\omega &\propto \omega_\circ^{1/2} \text{ when } R \approx R_c\,. \end{aligned} \tag{3.23}$$

Whether the dominant source of noise is the coil or the sample, the width of the resonance, and thus the bandwidth of the receiver, grows with MR frequency.[6]

The PMRI system uses a dual-mode transmit/receive coil. The transmit and receive modes differ by the function they perform in the MR circuitry. The transmit mode has to produce a high power (max 200 W) oscillating magnetic field in the direction perpendicular to the z-axis. This field causes the magnetization to tip away from the z-axis and, consequently, to precess like a spinning top around the readout field B_r. The transmit coil must have low Q (large $\Delta\omega$) so that it can recover quickly between subsequent RF pulses. To minimize distortion, the transmit coil's bandwidth has to be broader than the bandwidth of selective RF excitation pulses.

The receive mode of the RF circuitry has to detect and then amplify an *emf* signal on the order of a mV. Due to the small size of the detected signal, the receive coil must have a high Q for maximum SNR during acquisition and requires a low (typically 10 μW) power rating. In addition, the receive electronics must add minimum noise to the MR signal. To achieve this, an ultralow noise preamplifier is required. A tuned coil presents an impedance to the preamplifier that yields a low noise factor over 10 kHz bandwidth.

[6]This is valid only when resistance is in series with the inductor.

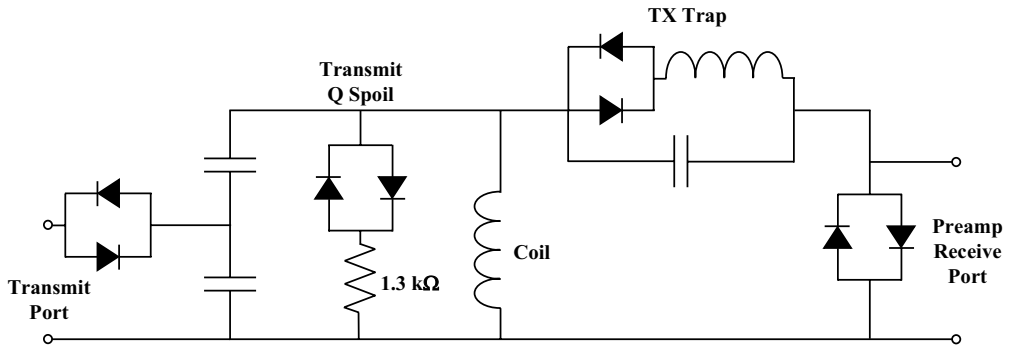

Figure 3.6: Dual transmit-receive circuit. The cross diodes present a short circuit in the transmit mode and an open circuit in the receive mode.

Figure 3.6 shows the schematics of the RF circuitry. The cross diodes can be regarded as switches that are *on* for voltages greater than 0.5 V, and *off* for other voltages. Since the transmitted signal is bigger than 0.5 V while the received signal is much smaller than 0.5 V, the diodes conduct in the transmit mode only, but present an open circuit in the receive mode. The pre-amplifier is thus protected from high voltages in the transmit mode. In addition, the coil's Q-factor is lowered during transmit mode by the presence of the 1.3 kΩ parallel resistor. For a resistor in parallel with the coil, the Q-factor is

$$Q = \frac{R}{\omega_\circ L} \,. \tag{3.24}$$

Contrary to Eq. 3.22, the Q-factor is now proportional to the total resistance. Since adding a resistor in parallel with the coil and sample resistances lowers the total resistance, the Q-factor is reduced.

Two type of coils were used in the prepolarized water and hyperpolarized gas experiments. A 9 cm diameter 4-turn litz wire saddle coil and a 3 cm diameter copper wire solenoid coil. Figure 3.7 shows the saddle coil, while Figure 3.8 shows the solenoid coil.

An RF slotted copper shield was added around the RF coils to shield them from the external magnetic fields which could degrade the coil's Q-factor. The shield slots, located where the coils RF image currents are zero, prevent gradient and polarizing coil eddy currents.

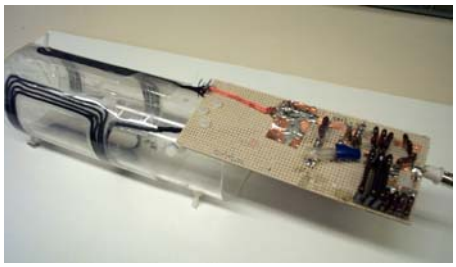

Figure 3.7: Saddle coil and the receiver-transmit circuitry used for hyperpolarized gas and water imaging at 1.1 MHz.

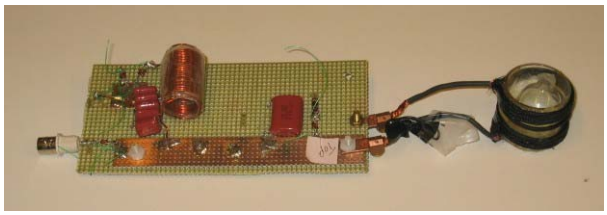

Figure 3.8: Solenoid coil and receiver-transmit circuitry used for hyperpolarized gas and water imaging at 397 kHz.

3.4.4 Gradients

The PMRI system, like the conventional MRI system, requires a 3-axis gradient coil to distinguish spin location in space. Due to the small bore required in PMRI imaging of the extremities, PMRI does not require high power gradient coils. The first gradient coil set was constructed using inexpensive cooper tape layered over an acrylic tube. The coils were 22.5 cm in diameter, 29 cm long, and at 10 A of current produced a gradient of 2.6 mT/m [25].

3.4.5 Techmag Console System - Data Acquisition and Control System

A commercial *Techmag Apollo* low-field imaging console was used in the experiments described in this work. *NTNMR* (version 1.3) software was used with the *Techmag* console. The software allowed the construction of various pulse sequences, such as gradient echo and spin echo sequences.

3.5 Hyperpolarized Gas Pumping Setup at Stanford

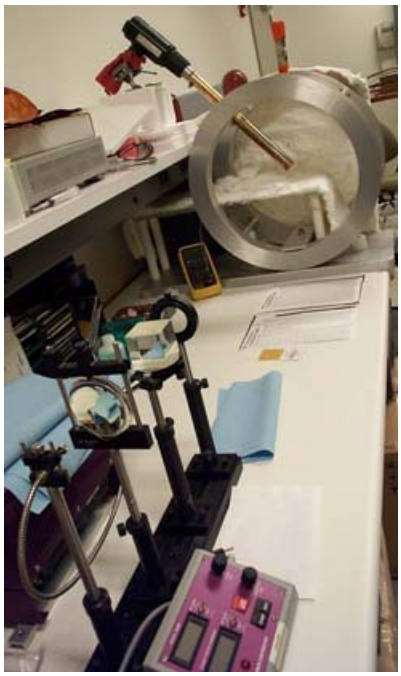

Figure 3.9: The pumping setup at Stanford.

The optical pumping setup at Stanford is displayed in Figure 3.9. The 1 inch cells were placed in the center of a 30 gauss field produced by a Helmholtz coil and heated by a heat gun to a temperature 120°C-150°C for ^{3}He and 80°C-90°C for ^{129}Xe. Optical pumping of Rb metal was achieved with approximately 7 W of circularly polarized laser light from a diode laser (15 W, *Optopower*, Tuscon, Arizona) that was tuned to the Rb D1 resonance (795 nm). The laser beam was first passed though a converging lens to prevent dispersion of the beam beyond the edges of the cell. It was then passed through a linear polarizer (i.e., beam-splitting cube) and through a quarter waveplate to produce circularly polarized laser light. Spin-exchange collisions between Rb electrons and the noble gas nuclei resulted in the hyperpolarization of the noble gas in the cell. The cell was then rapidly cooled in ice water to remove the Rb vapor by condensation onto the cell walls and so prevent depolarization of the hyperpolarized gas through collisions with unpolarized Rb atoms. Finally, the cell was carried into the low-field pulsed resistive scanner.

3.6 Concluding Remarks

Prepolarized MRI is a promising new MR technique which utilizes two variable electromagnets to produce low-field MR proton images, with SNR comparable to mid-field (0.5 T) scanners. The pulsed resistive low-field scanner has already produced high quality PMRI water images of human wrist anatomy [25].

In both, prepolarized MRI and hyperpolarized gas MRI, the amount of nuclear magnetization is independent of the readout field strength. There is thus no SNR advantage in increasing the readout field strength above the critical value at which the body becomes the dominant source of noise. The similarity of the prepolarized water and hyperpolarized gas SNR properties motivates the construction of a hybrid prepolarized water/hyperpolarized MR scanner [67].

In the next Chapter we are going to examine, among other things, whether the pulsed MR scanner is compatible with hyperpolarized gas imaging. In particular, we would like to know if the magnetic field is sufficiently stable for using spin echo based sequences, such as RARE, and whether the pulsing of the magnetic field destroys the hyperpolarized gas magnetization.